Draft version March 25, 2025
Typeset using LaTeX twocolumn style in AASTeX631

Helicity effect on turbulent passive and active scalar diffusivities

Axel Brandenburg,[1,2,3,4] Petri J. Käpylä,[5] Igor Rogachevskii,[6,1] and Nobumitsu Yokoi[7]

[1] Nordita, KTH Royal Institute of Technology and Stockholm University, Hannes Alfvéns väg 12, SE-10691 Stockholm, Sweden
[2] The Oskar Klein Centre, Department of Astronomy, Stockholm University, AlbaNova, SE-10691 Stockholm, Sweden
[3] McWilliams Center for Cosmology & Department of Physics, Carnegie Mellon University, Pittsburgh, PA 15213, USA
[4] School of Natural Sciences and Medicine, Ilia State University, 3-5 Cholokashvili Avenue, 0194 Tbilisi, Georgia
[5] Institut für Sonnenphysik (KIS), Georges-Köhler-Allee 401a, 79110 Freiburg im Breisgau, Germany
[6] Department of Mechanical Engineering, Ben-Gurion University of the Negev, P.O. Box 653, Beer-Sheva 84105, Israel
[7] Institute of Industrial Science, University of Tokyo, Komaba, Meguro, Tokyo 153-8505, Japan

ABSTRACT

Turbulent flows are known to produce enhanced effective magnetic and passive scalar diffusivities, which can fairly accurately be determined with numerical methods. It is now known that, if the flow is also helical, the effective magnetic diffusivity is reduced relative to the nonhelical value. Neither the usual second-order correlation approximation nor the various τ approaches have been able to capture this. Here we show that the helicity effect on the turbulent passive scalar diffusivity works in the opposite sense and leads to an enhancement. We have also demonstrated that the correlation time of the turbulent velocity field increases by the kinetic helicity. This is a key point in the theoretical interpretation of the obtained numerical results. Simulations in which helicity is being produced self-consistently by stratified rotating turbulence resulted in a turbulent passive scalar diffusivity that was found to be decreasing with increasing rotation rate.

Keywords: Astrophysical magnetism (102) — Magnetic fields (994)

1. INTRODUCTION

In many astrophysical plasmas such as stellar convection zones, the interstellar medium, and accretion discs, the Reynolds numbers are extremely large. Therefore, to describe the large-scale behavior of such flows, one often replaces the small viscosity or diffusion coefficients by effective ones. Turbulent diffusivities in the evolution equations for passive scalars act similarly as ordinary (molecular or atomic) ones, except that they characterize the diffusion of larger scale structures, as described by the corresponding averaged or coarse-grained evolution equations. Denoting the mean passive scalar concentration C by an overbar, the equation for $\overline{C}$ is given by

$$\frac{\partial\overline{C}}{\partial t} = -\boldsymbol{\nabla}\cdot\left(\overline{\boldsymbol{U}}\,\overline{C}\right) + (\kappa+\kappa_{\rm t})\nabla^2\overline{C}, \tag{1}$$

where we have allowed for the possibility of a mean flow $\overline{\boldsymbol{U}}$, while κ and $\kappa_{\rm t}$ are the microphysical and turbulent diffusion coefficients, respectively. The diffusion coefficients are proportional to the product of the mean free path and the typical velocity of particles or, in the turbulent case, the product of the integral turbulent scale and the rms velocity. Equation (1) is written for turbulence without stratification of the mean density or temperature, so that effective pumping velocity caused by the turbulent thermal diffusion vanishes (Elperin et al. 1997; Rogachevskii 2021).

The derivation of the turbulent diffusion coefficients is usually done by some approximations. Meanwhile, significant progress has been made by numerically computing these turbulent coefficients. A particularly useful approach is the test-field method (Schrinner et al. 2005, 2007), which was originally applied to magnetic fields in spherical geometry and then to Cartesian domains (Brandenburg 2005; Brandenburg et al. 2008). This method is sufficiently accurate to identify subtle effects caused by kinetic helicity in the flow (Brandenburg et al. 2017).

In the presence of magnetic fields, the kinetic helicity causes completely new qualities of its own. Unlike the case of turbulent or microphysical diffusion, helicity

brandenb@nordita.org

also produces non-diffusive effects that lead to a destabilization of the non-magnetic state. This is because helicity is a pseudo-scalar, which can couple the axial magnetic field vector with the polar electric field vector to give an extra contribution to the turbulent electromotive force in the mean-field induction equation. By contrast, the turbulent magnetic diffusivity is an ordinary scalar. It was therefore surprising when kinetic helicity was found to affect even the magnetic diffusivity (Brandenburg et al. 2017). This effect was such that helicity suppresses the magnetic diffusivity by a certain amount. The possibility of a helicity effect on the turbulent magnetic diffusivity was already noticed in the early work of Nicklaus & Stix (1988), but they found an enhancement of the turbulent magnetic diffusivity by the kinetic helicity.

Applying the Feynman diagram technique, Dolginov & Silant'ev (1987) show that kinetic helicity can increase the turbulent diffusion of a passive scalar field. On the other hand, subsequent work by Zhou (1990) using renormalization-group theory found no effect of helicity on the renormalized eddy viscosity. The effect of kinetic helicity on passive scalar diffusion was also investigated by Chkhetiani et al. (2006) using the renormalization group approach. They found that the effective diffusivity can be 50% larger in the helical case. They also noted that there is no helicity effect on the anomalous scaling of the structure functions.

The results of Brandenburg et al. (2017) were recently verified by Mizerski (2023) using the renormalization group approach. In particular, he found that for small magnetic Reynolds numbers, the helical correction to turbulent diffusion of the mean magnetic field is proportional to $\mathrm{Re}_\mathrm{M}^2 (H_\mathrm{K}\tau_\mathrm{c})^2/\langle\boldsymbol{u}^2\rangle$, where $\mathrm{Re}_\mathrm{M}=\tau_\mathrm{c}\,\langle\boldsymbol{u}^2\rangle/\eta$ is the magnetic Reynolds number, τ_c is the turbulent correlation time, η is the magnetic diffusion caused by an electrical conductivity of plasma, and $H_\mathrm{K}=\langle\boldsymbol{u}\cdot\boldsymbol{\omega}\rangle$ is the kinetic helicity. This scaling ($\propto \mathrm{Re}_\mathrm{M}^2$) is shown in Figure 4 of Brandenburg et al. (2017). This confirms that the helical correction cannot emerge from the second-order correlation approximation, where the transport coefficients are only linear in the magnetic Reynolds number.

What has not yet been specifically addressed is the effect of helicity on the passive scaler diffusivity, or even the thermal diffusivity of an active scalar such as the temperature or the specific entropy in the mean-field energy equation. Doing this is the purpose of the present work.

Helicity affects the value of the turbulent passive and active scalar diffusivity in a clear and consistent way. This is similar to the helicity effect on the turbulent magnetic diffusivity, but this new effect is the other way around, i.e., the turbulent passive and active scalar diffusion is enhanced by helicity, while the turbulent magnetic diffusivity is decreased. In the accompanying theoretical paper by Rogachevskii et al. (2025), remaining puzzles are addressed and possible explanations are being proposed.

Of some interest in this context is the earlier work of Brandenburg et al. (2012), who computed turbulent magnetic field and passive scalar transport for rotating stratified turbulence. The combined presence of rotation and stratification also leads to helicity and therefore to an α effect. They found a slight decrease of the magnetic diffusivity as the angular velocity is increased. At the time, this was not thought surprising because the focus was on new turbulent transport coefficients that only arise because of rotation and stratification. Furthermore, already rotation alone (without helicity) is known to decrease the turbulent magnetic diffusivity (Rädler et al. 2003).

For most astrophysical purposes, only order of magnitude estimates of turbulent transport coefficients are usually considered. This may change in future, when more accurate methods and measurements become more commonly available both in simulations and in observations. For example, the discrepancy in the estimate for the turbulent magnetic diffusivity was noticed in theoretical work in high-energy astrophysics on the chiral magnetic effect when simple estimates for the turbulent magnetic diffusivity did not match previous estimates (Schober et al. 2018). This discrepancy was then explained by the presence of helicity in one of the cases.

2. OUR MODEL

We consider both isothermal and non-isothermal turbulence and begin with the former.

2.1. *Basic equations for isothermal turbulence*

Our basic equations are the induction and passive scalar equations for the magnetic field $\boldsymbol{B}$ and the passive scalar concentration C (e.g., number density of particles). The magnetic field is also divergence-free. The governing equations are then

$$\frac{\partial \boldsymbol{B}}{\partial t} = \boldsymbol{\nabla}\times\left(\boldsymbol{U}\times\boldsymbol{B}-\boldsymbol{E}_\mathrm{diff}\right), \quad \boldsymbol{E}_\mathrm{diff}=-\eta\boldsymbol{\nabla}\times\boldsymbol{B}, \tag{2}$$

$$\frac{\partial C}{\partial t} = \boldsymbol{\nabla}\cdot\left(-\boldsymbol{U}C-\boldsymbol{F}_\mathrm{diff}\right), \quad \boldsymbol{F}_\mathrm{diff}=-\kappa\boldsymbol{\nabla}C. \tag{3}$$

The velocity $\boldsymbol{U}$ is obtained as a solution of the Navier-Stokes equations. In the kinematic test-field method, we ignore the feedback of the magnetic field on the flow, i.e., we solve

$$\frac{\mathrm{D}\boldsymbol{U}}{\mathrm{D}t} = -c_\mathrm{s}^2\boldsymbol{\nabla}\ln\rho+\boldsymbol{f}+\frac{1}{\rho}\boldsymbol{\nabla}\cdot(2\rho\nu\mathsf{S}), \tag{4}$$

$$\frac{\mathrm{D}\ln\rho}{\mathrm{D}t} = -\boldsymbol{\nabla}\cdot\boldsymbol{U}. \quad (5)$$

where ρ is the density, $c_{\rm s}$ is the isothermal sound speed, ν is the kinematic viscosity, S is the rate of strain tensor with the components $\mathsf{S}_{ij} = (\partial_i u_j + \partial_j u_i)/2 - \delta_{ij}\boldsymbol{\nabla}\cdot\boldsymbol{u}/3$, and $\boldsymbol{f}$ represents a forcing function that is δ-correlated in time and consists of plane waves with a mean forcing wavenumber $k_{\rm f}$. It is given by $f_i = R_{ij} f_j^{(\rm nohel)}$, where $R(\hat{\boldsymbol{k}}) = (\delta_{ij} - \sigma\epsilon_{ijk}\hat{k}_k)/\sqrt{1+\sigma^2}$ depends on $\hat{\boldsymbol{k}} = \boldsymbol{k}/k$ with $k = |\boldsymbol{k}|$ and the fractional helicity σ, and $\boldsymbol{f}^{(\rm nohel)} = f_0\,\boldsymbol{e}\times\boldsymbol{k}/|\boldsymbol{e}\times\boldsymbol{k}|$ is a nonhelical forcing function with f_0 being a scaling factor and $\boldsymbol{e}$ a random vector that is not aligned with $\boldsymbol{k}$.

2.2. *Equations for non-isothermal turbulence*

In our simulations of non-isothermal turbulence, we measure the response of the system to imposing large-scale gradient of specific entropy s with a relaxation time τ. The evolution equations for $\boldsymbol{u}$ and s are then

$$\frac{\mathrm{D}\boldsymbol{U}}{\mathrm{D}t} = -c_{\rm s}^2\boldsymbol{\nabla}(\ln\rho + s/c_{\rm p}) + \boldsymbol{f} + \frac{1}{\rho}\boldsymbol{\nabla}\cdot(2\rho\nu\mathsf{S}), \quad (6)$$

$$T\frac{\mathrm{D}s}{\mathrm{D}t} = 2\nu\mathsf{S}^2 + \frac{1}{\rho}\left(\boldsymbol{\nabla}\cdot\boldsymbol{F}_{\rm rad} - \mathcal{C}\right) - \frac{s-\tilde{s}_0}{\tau}, \quad (7)$$

where T is the temperature, $c_{\rm p}$ is the specific heat at constant pressure, $\boldsymbol{F}_{\rm rad} = -c_{\rm p}\rho\chi\boldsymbol{\nabla}T$ is the radiative flux, and $\mathcal{C}$ is a volumetric cooling function to compensate for viscous heating. Since the system is no longer isothermal, the sound speed is now given by $c_{\rm s}^2 = (\gamma-1)c_{\rm p}T$, where $\gamma = c_{\rm p}/c_{\rm v}$ is the ratio of specific heats, and $c_{\rm v}$ is the specific heat at constant volume. For the target profile of specific entropy, we choose $\tilde{s}_0 = s_0\sin k_T z$. Here, we take $k_T = k_1$ for what will later be called the test-field wavenumber, where $k_1 = 2\pi/L$ is the smallest wavenumber in the domain. Different values of k_T would be of interest for studying the scale dependence of turbulent transport, as has been done on various occasions (Brandenburg & Sokoloff 2002; Brandenburg et al. 2008, 2009).

2.3. *Parameters*

For the scale separation ratio, i.e., the ratio of the forcing wavenumber $k_{\rm f}$ and the box wavenumber k_1, we take $k_{\rm f}/k_1 = 5.1$ in most of our cases. Although not stated explicitly there, this was also the value adopted in Brandenburg et al. (2017). Larger (smaller) values of $k_{\rm f}$ allow us to access larger (smaller) scale separation ratios. At the end of this paper, we present a small survey of different choices; see also Brandenburg et al. (2008, 2009) for such studies in other contexts. Our main governing control parameters are the Reynolds number $\mathrm{Re} = u_{\rm rms}/\nu k_{\rm f}$ and the Mach number $\mathrm{Ma} = u_{\rm rms}/c_{\rm s}$. The Schmidt number, $\mathrm{Sc} = \nu/\kappa$, the magnetic Prandtl number, $\mathrm{Pr_M} = \nu/\eta$, and the thermal Prandtl number $\mathrm{Pr} = \nu/\chi$ are unity in all cases. Therefore, the magnetic Reynolds number $\mathrm{Re_M} = u_{\rm rms}/\eta k_{\rm f}$ and the Péclet number $\mathrm{Pe} = u_{\rm rms}/\chi k_{\rm f}$ equal the fluid Reynolds number in all cases.

2.4. *Test-field methods*

The test-field method implies the simultaneous solution of additional equations for the fluctuating magnetic field or the fluctuating passive scalar concentration. The variables are indicated by the letter T. The equations are obtained by subtracting the corresponding averaged equations from the original ones and yield

$$\frac{\partial\boldsymbol{b}^T}{\partial t} = \boldsymbol{\nabla}\times\left(\boldsymbol{u}\times\overline{\boldsymbol{B}}^T + \overline{\boldsymbol{U}}\times\boldsymbol{b}^T + \boldsymbol{\mathcal{E}}'_T\right) + \eta\nabla^2\boldsymbol{b}^T, \quad (8)$$

$$\frac{\partial c^T}{\partial t} = \boldsymbol{\nabla}\cdot\left(-\boldsymbol{u}\overline{C}^T - \overline{\boldsymbol{U}}c^T + \boldsymbol{\mathcal{F}}'_T\right) + \kappa\nabla^2 c^T, \quad (9)$$

where $\boldsymbol{\mathcal{E}}'_T = \boldsymbol{u}\times\boldsymbol{b} - \overline{\boldsymbol{u}\times\boldsymbol{b}}$ and $\boldsymbol{\mathcal{F}}'_T = -(\boldsymbol{u}c - \overline{\boldsymbol{u}c})$ are nonlinear terms that are neglected in the second-order correlation approximation. Including those terms yields the new subtle effects that we found in Brandenburg et al. (2017) for $\eta_{\rm t}$ and in the present work for $\kappa_{\rm t}$.

In the following, we assume planar averages and denote them by overbars, e.g., $\overline{\boldsymbol{B}}(z,t) = \int \boldsymbol{B}(x,y,z,t)\,\mathrm{d}z/L_\perp^2$, where $L_\perp$ is the extent of the computational domain in the xy plane. In the spirit of the test-field method, one decouples Equations (8) and (9) from those for the actual fluctuations and solve them for a set of mean fields (mean scalars) such that one can compute α_{ij}, η_{ij}, and κ_{ij} uniquely for each time step and at each value of z. Using as a shorthand $s = \sin k_T z$ and $c = \cos k_T z$, we choose sinusoidal and cosinusoidal test fields $\overline{\boldsymbol{B}}^1 = (s,0,0)$, $\overline{\boldsymbol{B}}^2 = (c,0,0)$, $\overline{\boldsymbol{B}}^3 = (0,s,0)$, and $\overline{\boldsymbol{B}}^4 = (0,c,0)$, as well as $\overline{C}^1 = s$, $\overline{C}^2 = c$, i.e., four different test fields for $\overline{\boldsymbol{B}}^T$ and two different ones for $\overline{C}^T$. This allows us to compute the coefficient α_{ij}, η_{ij}, and κ_{ij} in the parameterizations

$$\overline{\mathcal{E}}_i^T = \alpha_{ij}\overline{B}_j^T - \eta_{ij}(\boldsymbol{\nabla}\times\overline{\boldsymbol{B}}^T)_j, \quad (10)$$

$$\overline{\mathcal{F}}_i^T = \gamma_i\overline{C}^T - \kappa_{ij}\nabla_j\overline{C}^T, \quad (11)$$

where $\overline{\boldsymbol{\mathcal{E}}}^T = \overline{\boldsymbol{u}\times\boldsymbol{b}_T}$, $\overline{\boldsymbol{\mathcal{F}}}^T = -\overline{\boldsymbol{u}c_T}$, and $i,j = 1,2$ denote the x and y components. The aforementioned turbulent viscosity and passive scalar diffusivity are then given by $\eta_{\rm t} = (\eta_{11} + \eta_{22})/2$ and $\kappa_{\rm t} = (\kappa_{11} + \kappa_{22})/2$. The effective pumping velocity $\boldsymbol{\gamma}$ of the mean magnetic field vanishes for homogeneous turbulence, but the effective pumping velocity $\boldsymbol{\gamma}$ of the mean passive scalar field due to the density stratification of the fluid (Elperin et al.

1997; Rogachevskii 2021) was found to lead to downward transport of the mean passive scalar concentration (to the maximum of the mean fluid density) in density stratified turbulence (Brandenburg et al. 2012; Haugen et al. 2012).

It should be noted that in the original application of the test-field method, Schrinner et al. (2005, 2007) used a combination of constant and linearly varying test fields. This choice is appropriate for computing turbulent transport properties on the largest possible scales, but it is not well suited for the use in periodic domains. This was the main reason why Brandenburg (2005) employed sinusoidal and cosinusoidal test fields, but it also provided a natural way of computing the dependence of the turbulent transport coefficients on different length scales or for different wavenumbers. The resulting formulation of the electromotive force in Fourier space translates directly into one in terms of integral kernels (Brandenburg et al. 2008). This allowed us to avoid the restriction to large scale separation in space and time by replacing the multiplications with turbulent transport coefficients by a convolution with the appropriate integral kernels; see Hubbard & Brandenburg (2009) and Rheinhardt & Brandenburg (2012) for corresponding studies. The effect of different spatial scales on turbulent mixing was also investigated by de Avillez & Mac Low (2002) using checkerboard patterns, but this approach cannot so easily be utilized in the framework of mean-field theory.

2.5. *Active scalar diffusivity*

To determine the turbulent radiative diffusion coefficient, we use the standard mean-field expression for the enthalpy flux (Rüdiger 1989),

$$\overline{\boldsymbol{\mathcal{F}}}_{\rm enth} = -\chi_{\rm t}\overline{\rho}\overline{T}\boldsymbol{\nabla}\overline{S}, \qquad (12)$$

where the actual enthalpy flux is computed as $\overline{\boldsymbol{\mathcal{F}}}_{\rm enth} = \overline{(\rho\boldsymbol{U})' c_{\rm p} T'}$, and correlate their z components against each other to determine $\chi_{\rm t}$. Here, primes denote the departures from the horizontal means. This method follows that employed by Käpylä & Singh (2022), who also computed the turbulent kinematic viscosity in an analogous way be correlating the yz component of the Reynolds stress against the corresponding component of the mean-field strain tensor. The current setup differs from that in Käpylä & Singh (2022) in that a large-scale velocity is not imposed and therefore no off-diagonal Reynolds stress is present. The emergence of such off-diagonal components in shear flows was studied by Mitra et al. (2009), who found an increase of the turbulent magnetic diffusivity.

2.6. *Simulations, data, and error bars*

We use the Pencil Code for our simulations (Pencil Code Collaboration et al. 2021). It uses sixth order accurate spatial derivatives and a third order timestepping scheme. It also allows us to compute turbulent transport coefficients with the test-field method. For that purpose, we invoke the modules `testfield_z` and `testscalar` within the Pencil Code.

We present our results for α, $\eta_{\rm t}$, and $\kappa_{\rm t}$ in normalized form and divide α by $A_0 = u_{\rm rms}/3$ and $\eta_{\rm t}$ and $\kappa_{\rm t}$ by $D_0 = u_{\rm rms}/3k_{\rm f}$. This allows us to compare runs with different rms velocity amplitudes.

Our results for the turbulent transport coefficients are functions of z and t. Since the turbulence in our simulations is homogeneous, we average the resulting transport coefficients over z. The resulting time series is then averaged over statistically steady intervals and error bars have been estimated by taking the largest departure to the average from any one third of the full time series. For sufficiently long time series, the resulting errors are rather small, so we often exaggerate them by a factor of 3 or 4, as is indicated in the plots below.

3. RESULTS

3.1. *Passive scalar results and comparison*

Although the results for $\eta_{\rm t}$ have already been computed in Brandenburg et al. (2017), we compute them here again by invoking similar test-field routines in the Pencil Code at the same time. The test-field method for passive scalars was already described in Brandenburg et al. (2009). Rädler et al. (2011) applied it to passive scalar diffusion in compressible flows. In the following, we use $u_{\rm rms}$ and $k_{\rm f}$ to express our results in nondimensional form by normalizing the diffusivities by $u_{\rm rms}/3k_{\rm f}$. Using earlier test-field results, this was found to be an accurate estimate (Sur et al. 2008).

Figure 1 shows a comparison of time series of $\kappa_{\rm t}$ and $\eta_{\rm t}$ for nonhelical and helical cases and $\mathrm{Re} = 2.4$. While $\kappa_{\rm t}$ appears to be unaffected by the presence of helicity, $\eta_{\rm t}$ is suppressed, as already found by Brandenburg et al. (2017). For $\mathrm{Re} = 120$, however, $\kappa_{\rm t}$ is found to be *enhanced* by the presence of helicity; see Figure 2. We have considered a number of additional simulations with other values of Re. The dependence on Re is shown in Figure 3; see also Table 1 for a summary. The trend in $\eta_{\rm t}$ does not follow a smooth dependence, suggesting that statistical noise or other unaccounted factors may have influenced the results.

The forcing is kept constant between different runs, so the resulting rms velocity depends on how stiff the system is against this forcing. We see that the value of the Mach number increases slightly with increasing values of the Reynolds number. We also see that the Mach num-

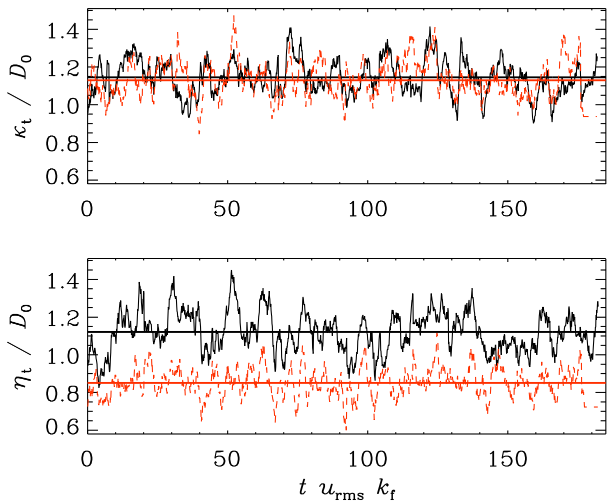

Figure 1. Time series of κ_t (upper panel) and η_t (lower panel) for Runs A without helicity (solid black line) and with helicity (dashed red line) with $\mathrm{Re} = 2.4$. The thick black and red horizontal lines denote the time-averaged values.

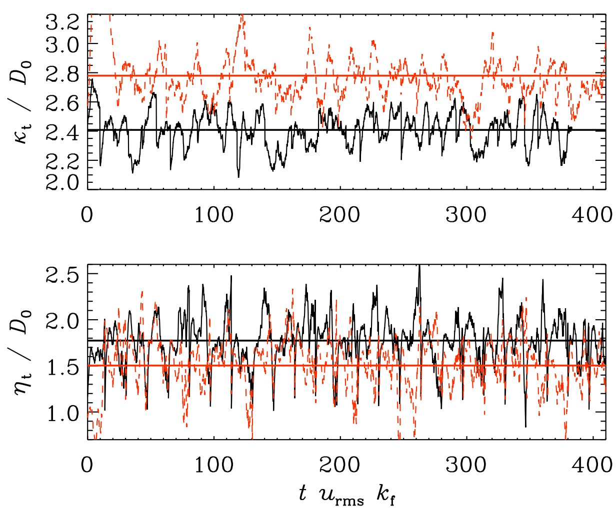

Figure 2. Similar to Figure 1, but for Runs F with $\mathrm{Re} = 120$.

ber is slightly enhanced in the simulations with helical forcing. This suggests that such flows are less effective in dissipating energy. These slight changes in Ma do not significantly affect our results for η_t and κ_t, because we always present our results in normalized form and we are here only interested in subsonic turbulence. Note also that the compressibility of the turbulence affects only non-helical contributions to the turbulent diffusion (Rogachevskii et al. 2018).

In Appendix A, we compare our results with different degrees of helicity with earlier simulations of rotating stratified turbulence in which helicity is automatically being produced in self-consistent way. It turns out, however, that the enhancement of turbulent diffusion by helicity is not being reproduced in such simulations. We argue that this is caused by the more dominant effect of rotation which strongly suppresses turbulent transport.

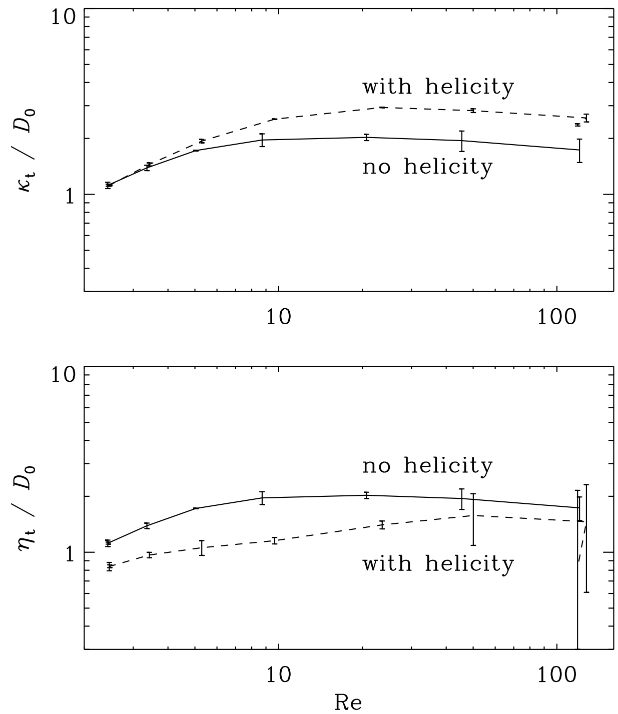

Figure 3. Reynolds number dependence of κ_t (upper panel) and η_t (lower panel) for nonhelical (solid lines) and helical (dashed lines). The error bars have been exaggerated by a factor of 3.

3.2. *Active scalar results*

The results of simulations similar to those of Käpylä & Singh (2022) are shown in Figure 4. Here we see the turbulent heat diffusivity computed from an imposed entropy gradient (see Käpylä & Singh 2022, for details) for non-helical and helical cases. For $\mathrm{Pe} = \mathrm{Re} > 10$, there is a statistically significant increase of χ_t by about 10% for the helical cases relative to the nonhelical ones. These results were obtained by correlating the actual enthalpy flux with the mean-field expression given by Equation (12). In Käpylä & Singh (2022), an alternative independent method was used where the mean entropy profile is initially forced and then allowed to decay. This yielded very similar results.

The kinetic helicity effects on turbulent diffusion of the mean magnetic and scalar fields are partially related to the helicity effect on the effective correlation time. To examine this in more detail, we compute the correlation

Table 1. Values of $\kappa_{\rm t}^{\rm nhel}$ and $\kappa_{\rm t}^{\rm hel}$ as well as $\eta_{\rm t}^{\rm nhel}$ and $\eta_{\rm t}^{\rm hel}$, normalized by $D_0 \equiv u_{\rm rms}/3k_{\rm f}$, for the nonhelical and helical cases, and $\alpha^{\rm hel}$ normalized by $A_0 \equiv u_{\rm rms}/3$, for the helical cases for different values of Re. The value of Ma is given for completeness.

Run	Re	$\kappa_{\rm t}^{\rm nhel}/D_0$	$\kappa_{\rm t}^{\rm hel}/D_0$	$\eta_{\rm t}^{\rm nhel}/D_0$	$\eta_{\rm t}^{\rm hel}/D_0$	$\alpha^{\rm hel}/A_0$	$\rm Ma^{nhel}$	$\rm Ma^{hel}$
A	2.4	1.14 ± 0.01	1.12 ± 0.01	1.12 ± 0.01	0.84 ± 0.015	-0.83 ± 0.01	0.062	0.063
B	3.4	1.47 ± 0.03	1.45 ± 0.03	1.39 ± 0.02	0.97 ± 0.011	-0.95 ± 0.02	0.068	0.070
C	5.0	1.87 ± 0.04	1.93 ± 0.04	1.72 ± 0.00	1.06 ± 0.03	-1.02 ± 0.02	0.077	0.081
D	8.7	2.26 ± 0.03	2.54 ± 0.01	1.96 ± 0.05	1.15 ± 0.02	-0.96 ± 0.01	0.089	0.099
E	20.7	2.54 ± 0.02	2.94 ± 0.01	2.03 ± 0.03	1.40 ± 0.02	-0.83 ± 0.02	0.105	0.120
F	45.5	2.50 ± 0.03	2.82 ± 0.07	1.95 ± 0.08	1.58 ± 0.16	-0.75 ± 0.03	0.116	0.128
G	120.6	2.27 ± 0.01	2.58 ± 0.12	1.73 ± 0.08	1.46 ± 0.28	-0.69 ± 0.07	0.123	0.130

Table 2. Values of $\chi_{\rm t}^{\rm nhel}$ and $\chi_{\rm t}^{\rm hel}$ normalized by $D_0 \equiv u_{\rm rms}/3k_{\rm f}$, for the nonhelical and helical cases. The value of Ma is given for completeness.

Run	Re	$\chi_{\rm t}^{\rm nhel}/D_0$	$\chi_{\rm t}^{\rm hel}/D_0$	Ma
A	1.2	0.63 ± 0.03	0.59 ± 0.02	0.031
B	4.7	1.86 ± 0.08	1.78 ± 0.09	0.048
C	11.8	2.51 ± 0.05	2.72 ± 0.07	0.060
D	27.6	2.57 ± 0.01	2.95 ± 0.07	0.070
E	75.1	2.40 ± 0.03	2.67 ± 0.04	0.077
F	151.9	2.25 ± 0.02	2.52 ± 0.04	0.077
G	307.0	2.18 ± 0.04	2.42 ± 0.05	0.078

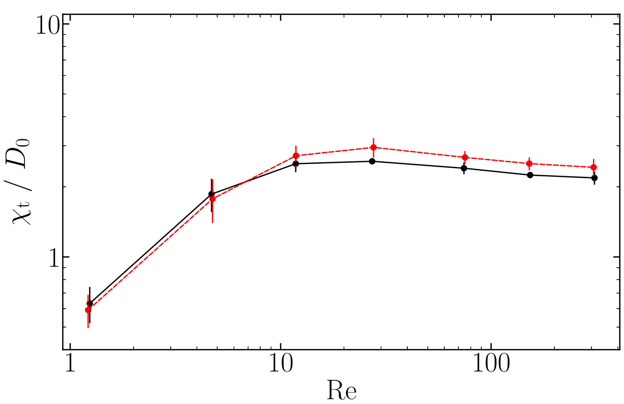

Figure 4. Dependence of $\chi_{\rm t}$ for nonhelical (black symbols, solid line) and fully helical turbulence (red symbols, dashed line) as a function of Reynolds number $\mathrm{Re} = \mathrm{Pe}/\mathrm{Pr}$ with $\mathrm{Pr} = 1$ in all cases. To make the error bars more visible, they have been exaggerated by a factor of 4.

times as the late-time limit of

$$\tau_{\rm c}(t) = \int_{t_0}^{t} \langle \boldsymbol{u}(t_0) \cdot \boldsymbol{u}(t') \rangle \, {\rm d}t' \bigg/ \left\langle \boldsymbol{u}^2(t_0) \right\rangle . \tag{13}$$

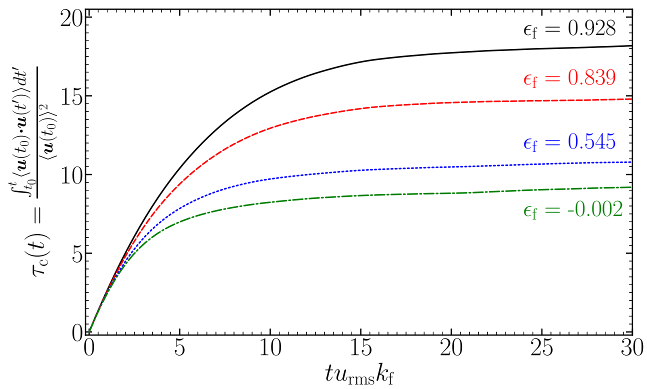

Figure 5. Correlation time of turbulence computed from time integrals of velocity autocorrelation from runs with $\mathrm{Re} = 13$ and different relative helicity $\epsilon_{\rm f} = \langle \boldsymbol{u} \cdot \boldsymbol{\omega} \rangle / k_{\rm f} u_{\rm rms}^2$.

The result is shown in Figure 5 for simulations with $\mathrm{Re} = 13$ and different values of the relative helicity. We see that, through the presence of kinetic helicity, the correlation time of the turbulent velocity field increases and is more than doubled as the kinetic helicity is increased from zero to one. We note that the Reynolds number of these simulations is very modest. Further studies at larger Reynolds numbers would be needed to establish the dependence of the correlation time on the kinetic helicity in more turbulent regimes; see Rogachevskii et al. (2025).

Another way to estimate the correlation time is obtained from the ratio of kinetic energy and its dissipation rate:

$$\tau_{\rm c} = \frac{E_{\rm K}}{\epsilon_{\rm K}}, \tag{14}$$

where $E_{\rm K} = \frac{1}{2}\langle \boldsymbol{u}^2 \rangle$ and $\epsilon_{\rm K} = 2\nu \langle \mathbf{S}^2 \rangle$. The results for the correlation time are summarized in Figure 6. Both measures of $\tau_{\rm c}$ show an increasing trend as a function of the fractional helicity, $\epsilon_{\rm f} = \overline{\boldsymbol{u} \cdot \boldsymbol{\omega}} / k_{\rm f} u_{\rm rms}^2$.

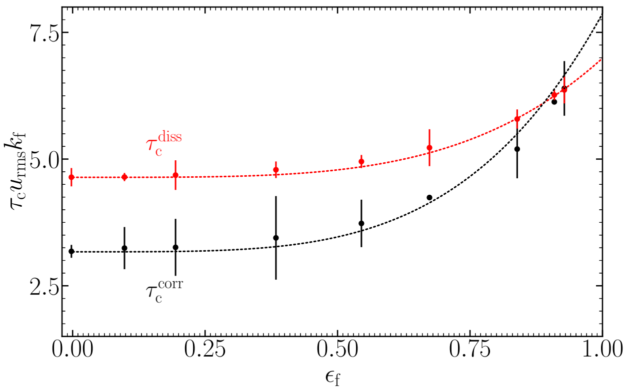

Figure 6. Correlation time τ_c as function of ϵ_f from the late-time limit of Equation (13) (black symbols) and from Equation (14) (red symbols) normalized by the turnover time $(u_{\rm rms} k_f)^{-1}$ for the same runs as in Figure 5. The dotted lines are proportional to ϵ_f^4, and the error bars are boosted by a factor of ten for $\tau_c^{\rm diss}$ and by five for $\tau_c^{\rm corr}$.

Regarding the usage of the energy dissipation rate ϵ_K for the timescale arguments of turbulence, we should note the following points. Although developed turbulence contains a very wide range of scales, it is still meaningful to use ϵ_K for the arguments of turbulence timescale. In the inertial range of fully developed turbulence, we have a local equilibrium between the production rate of turbulent energy and its dissipation rate. In this range, the dissipation rate is equivalent both to the energy injection rate at the integral scale and to the energy flux (the spectral energy transfer from larger scale to smaller scale). In this sense, the energy dissipation rate ϵ_K is the most appropriate turbulence statistical quantity that describes the timescale of turbulence. This is the reason why we also adopt ϵ_K in the timescale argument of turbulence.

Turbulent transport coefficients depend on some statistical quantities such as the turbulent energy E_K, its dissipation rate ϵ_K, kinetic helicity H_K, etc, as well as the time and/or length scales of turbulence, which are determined by E_K, ϵ_K and H_K, as well as the velocity strain rate, vorticity, pressure, etc. Generally, the kinetic helicity H_K depends on the vorticity/rotation and density stratification or turbulence inhomogeneity as well as the external forcing. Here, for simplicity of the argument, we assume that deviations of the turbulence timescale from the usual eddy turnover time, $\tau_c = E_K/\epsilon_K$, can be expressed in terms of the kinetic helicity as $\tau_c(H_K)$, and examine the dependence of τ_c on H_K.

3.3. *Comparisons with the theoretical predictions*

Let us compare the obtained numerical results with the theoretical predictions by Rogachevskii et al. (2025), where the path-integral approach for a random velocity field with a finite correlation time has been used. According to the theory, the turbulent magnetic diffusion coefficient $\eta_t(H_K)$ is given by

$$\eta_t(H_K) = \eta_{t0} \, \frac{\tau_c(H_K)}{\tau_0} \left(1 - \frac{\tau_c^2(H_K)}{3} \, \frac{H_K^2}{\langle \boldsymbol{u}^2 \rangle}\right), \quad (15)$$

while the turbulent diffusion coefficient $\kappa_t(H_K)$ of the scalar field is

$$\kappa_t(H_K) = \kappa_{t0} \, \frac{\tau_c(H_K)}{\tau_0} \left(1 - \frac{\tau_c^2(H_K)}{6} \, \frac{H_K^2}{\langle \boldsymbol{u}^2 \rangle}\right), \quad (16)$$

where $H_K = \langle \boldsymbol{u} \cdot \boldsymbol{\omega} \rangle$, $\eta_{t0} = \eta_t(H_K = 0)$, $\kappa_{t0} = \kappa_t(H_K = 0)$ and $\tau_0 = \tau_c(H_K = 0) = (u_{\rm rms} k_f)^{-1}$. Applying two independent methods (based on the non-instantaneous correlation functions and the rate of energy dissipation) for the calculation of the correlation time versus the fraction of kinetic helicity, our numerical results suggest that

$$\tau_c(H_K)/\tau_0 \approx 1 + 0.5\epsilon_f^4. \quad (17)$$

Using Equations (15)–(17), we plot in Figure 7 the dependences $\eta_t(0) - \eta_t$ and $\kappa_t(0) - \kappa_t$ on the fraction ϵ_f of the kinetic helicity for Re $= 13$. Here, $\eta_t(0) = \eta_t(\epsilon_f = 0)$ and $\kappa_t(0) = \kappa_t(\epsilon_f = 0)$, and α is normalized by $A_0 = u_{\rm rms}/3$, while turbulent diffusion coefficients are normalized by $D_0 = u_{\rm rms}/3k_f$, where k_f is the forcing wavenumber. The theoretical dependencies given by Equations (15)–(17) are shown as dashed and dotted blue and black curves. The theoretical results for $\epsilon_f \gtrsim 0.85$ are shown as dotted lines, because they may not be reliable.

As follows from Figure 7, the turbulent magnetic diffusion coefficient is reduced by the kinetic helicity, while the turbulent diffusion coefficient for the scalar field is increased by the kinetic helicity. These arguments can explain the results of our direct numerical simulations; see also Fig. 1 for Re $= 120$ in Rogachevskii et al. (2025).

Using an approach based on the Furutsu-Novikov theorem (Furutsu 1963; Novikov 1965), Kishore & Singh (2025) found that the turbulent diffusivities of both the mean passive scalar and the mean magnetic field are suppressed by the kinetic helicity. Note that Kishore & Singh (2025) have not taken into account the dependence of the correlation time on the kinetic helicity. This may explain the discrepancy with our numerical results related to the helicity effect on turbulent diffusion of the scalar fields.

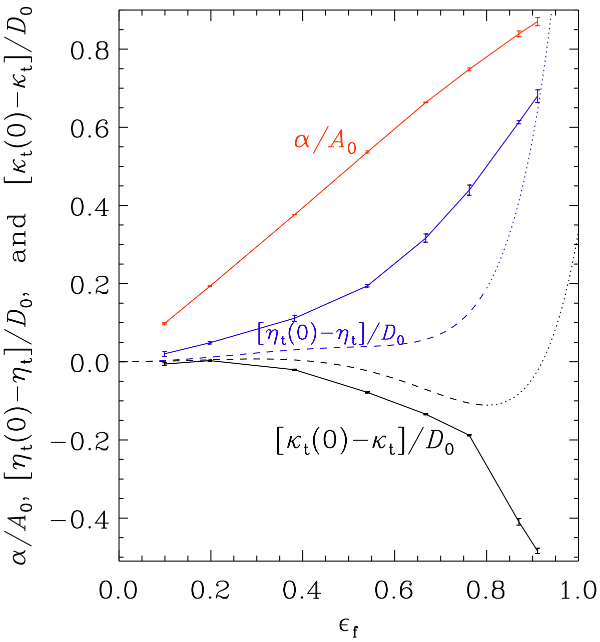

Figure 7. Dependencies of α (red solid line), $\eta_{\rm t}(0)-\eta_{\rm t}$ (blue solid line) and $\kappa_{\rm t}(0)-\kappa_{\rm t}$ (black solid line) on the fraction $\epsilon_{\rm f}$ of the kinetic helicity for Re $=13$. The theoretical dependencies given by Equations (15)–(17) are shown by dashed and dotted blue and black curves. The theoretical results for $\epsilon_{\rm f}\gtrsim 0.85$ are shown as dotted lines, because they may not be reliable.

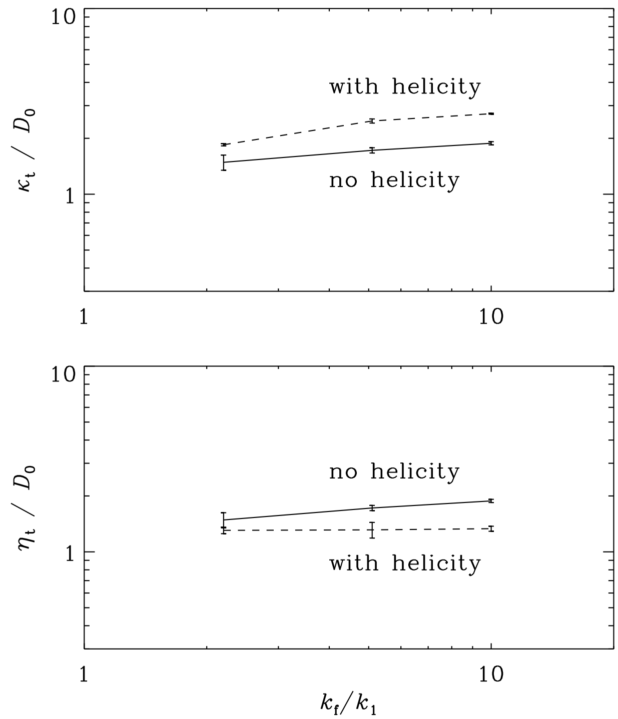

Figure 8. Scale separation dependence of $\kappa_{\rm t}$ (upper panel) and $\eta_{\rm t}$ (lower panel) for nonhelical (solid lines) and helical (dashed lines). To make the error bars more visible, they have been exaggerated by a factor of 4.

3.4. *Scale dependence*

To assess the scale dependence of the difference of turbulent transport for helical and nonhelical cases, we have varied the ratio $k_{\rm f}/k_1$, keeping the viscosity constant. This implies that Re decreases with increasing $k_{\rm f}$. In all cases, we used 512^3 meshpoints. The results for helical and nonhelical turbulence are compared in Figure 8 and Table 3. We see that there is a slight increase in the difference between helical and nonhelical cases. For $\kappa_{\rm t}$, however, the difference between helical and nonhelical cases is rather weak. In all cases, we used 512^3 meshpoints.

4. CONCLUSIONS

Our simulations have revealed a surprising difference in the helicity effect for passive and active scalars on the one hand and magnetic fields on the other. As for magnetic fields, the helicity effect does not exist for small Reynolds numbers. Above Reynolds numbers of about 20, it does not change much any more and there is no indication that it disappears at larger values.

The key numerical result of the present study is the enhancement of turbulent diffusion of the mean passive and active scalar fields by the kinetic helicity. This result is opposite to the magnetic case where turbulent magnetic diffusion is decreased by the kinetic helicity. We also found that the correlation time of the turbulent velocity field increases because of kinetic helicity. The latter is one of the main points relevant for understanding the kinetic helicity effects on turbulent diffusion of scalar and magnetic fields (see Section 3.3).

The enhancement of the passive scalar diffusion examined here can be compared with the effect of rotation and stratification on the passive scalar diffusivity. As discussed in the introduction, rotating stratified flows also attain kinetic helicity and for such flows, it was previously found that the passive scalar diffusivity gets reduced as the rotation speed is increased, just like the magnetic diffusivity, which also became smaller (Brandenburg et al. 2012). This effect was not ascribed to the presence of helicity, but it was simply regarded as a rotational suppression of the magnetic diffusivity. This difference can probably be explained by the anisotropy of the flow that is being produced in rotating stratified turbulence, which is a more complicated situation than just a helically forced flow.

Qualitatively, one could understand the helicity effect on the magnetic field as a tendency to support dynamo action, or, alternatively, as a tendency for rotational suppression of the magnetic diffusivity. For pas-

Table 3. Values of $\kappa_\mathrm{t}^\mathrm{nhel}$ and $\kappa_\mathrm{t}^\mathrm{hel}$ as well as $\eta_\mathrm{t}^\mathrm{nhel}$ and $\eta_\mathrm{t}^\mathrm{hel}$, normalized by $D_0 \equiv u_\mathrm{rms}/3k_\mathrm{f}$, for the nonhelical and helical cases, and α^hel normalized by $A_0 \equiv u_\mathrm{rms}/3$, for the helical cases for different values of k_f. The value of Ma is given for completeness.

Run	k_f/k_1	Re	$\kappa_\mathrm{t}^\mathrm{nhel}/D_0$	$\kappa_\mathrm{t}^\mathrm{hel}/D_0$	$\eta_\mathrm{t}^\mathrm{nhel}/D_0$	$\eta_\mathrm{t}^\mathrm{hel}/D_0$	α^hel/A_0	$\mathrm{Ma}^\mathrm{nhel}$	Ma^hel
a	2.2	281.1	1.66 ± 0.03	1.85 ± 0.03	1.49 ± 0.14	1.31 ± 0.05	-0.65 ± 0.01	0.125	0.131
b	5.1	120.6	2.27 ± 0.01	2.48 ± 0.06	1.72 ± 0.06	1.31 ± 0.13	-0.69 ± 0.01	0.123	0.130
c	10.0	59.3	2.49 ± 0.01	2.71 ± 0.02	1.88 ± 0.04	1.33 ± 0.04	-0.76 ± 0.00	0.119	0.129

sive and active scalars, on the other hand, there is no dynamo effect. Furthermore, in some special deterministic flows (the Roberts-IV flow; see Devlen et al. (2013)), the effective magnetic diffusivity can even be negative and thereby lead to dynamo action. Such an effect was never found for passive or active scalars or magnetic fields in turbulent flows at high Reynolds numbers. What has been previously found, however, is a suppression of both η_t and κ_t for potential (compressible) flows (Rädler et al. 2011; Rogachevskii et al. 2018). In the present work, however, we have only considered nearly incompressible flows for actual turbulence simulations, as opposed to some constructed flows such as the Roberts flow.

We thank Nathan Kleeorin for useful discussions and the referees for their reports. We also acknowledge the discussions with participants of the Nordita Scientific Program on "Stellar Convection: Modelling, Theory and Observations", Stockholm (September 2024). This research was supported in part by the Swedish Research Council (Vetenskapsrådet) under Grant No. 2019-04234, the National Science Foundation under grant no. NSF AST-2307698, a NASA ATP Award 80NSSC22K0825, and the Munich Institute for Astro-, Particle and BioPhysics (MIAPbP), which is funded by the Deutsche Forschungsgemeinschaft (DFG, German Research Foundation) under Germanys Excellence Strategy - EXC-2094 - 390783311. Part of this work was supported by the Japan Society of the Promotion of Science (JSPS) Grants-in-Aid for Scientific Research JP23K25895. We acknowledge the allocation of computing resources provided by the Swedish National Allocations Committee at the Center for Parallel Computers at the Royal Institute of Technology in Stockholm, and by the North German Supercomputing Alliance (HLRN) in Göttingen and Berlin, Germany.

Software and Data Availability. The source code used for the simulations of this study, the Pencil Code (Pencil Code Collaboration et al. 2021), is available on https://github.com/pencil-code/. The simulation setups and corresponding secondary data are available on http://doi.org/10.5281/zenodo.15083000.

APPENDIX

A. COMPARISON WITH EARLIER WORK

In Figure 9, we compare with the values of the α effect and the turbulent magnetic and passive scalar diffusivities from the earlier work of Brandenburg et al. (2012), in which kinetic helicity is being produced by the interaction with rotation and stratification. Here, we have estimated the fractional helicity from the product of Coriolis number $\mathrm{Co} = 2\Omega/u_\mathrm{rms}k_\mathrm{f}$ and gravity number $\mathrm{Gr} = 1/H_\rho k_\mathrm{f}$, where Ω is the angular velocity, k_f is the forcing wavenumber of the turbulence, and H_ρ is the density scale height. We used a formula by Jabbari et al. (2014), $\epsilon_\mathrm{f} = 2\,\mathrm{Co}\,\mathrm{Gr}$. For the present simulations, we used $\epsilon_\mathrm{f} \approx 2\sigma/(1+\sigma^2)$.

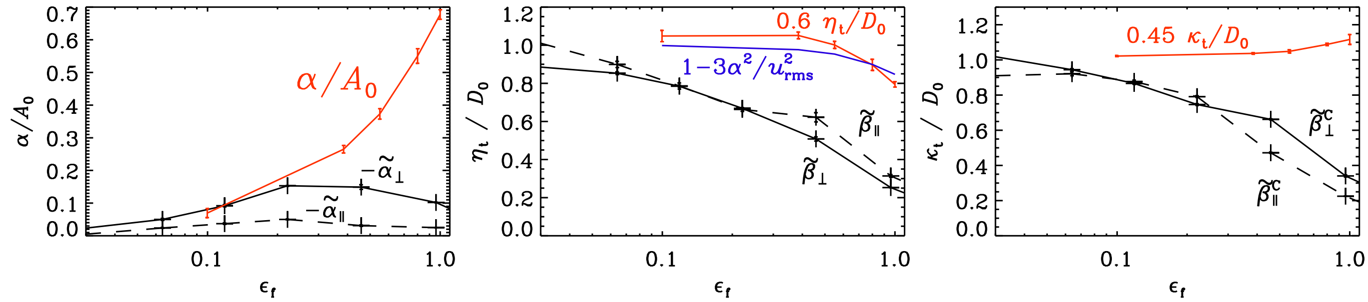

Figure 9. Dependence of the fractional helicity, $\epsilon_{\rm f}$, and comparison of the values of α and the turbulent magnetic and passive scalar diffusivities with the earlier work of Brandenburg et al. (2012), in which kinetic helicity is being produced by the interaction with rotation and stratification. The originally used symbols of Brandenburg et al. (2012) have been retained: $-\tilde{\alpha}_\perp$ and $-\tilde{\alpha}_\parallel$ for the normalized perpendicular and parallel components of the α effect, $\tilde{\beta}_\perp$ and $\tilde{\beta}_\parallel$ for those of the magnetic diffusivity, and $\tilde{\beta}_\perp^{\rm C}$ and $\tilde{\beta}_\parallel^{\rm C}$ for those of the passive scalar diffusivity. The tildes indicate appropriate normalization. In the second panel, we also show in blue $1-3\alpha^2/u_{\rm rms}^2$.

There is not much agreement with our present simulations, shown in red. This shows that other effects such as the rotational suppression of turbulent transport plays a more dominant role than just the helicity.

REFERENCES

Brandenburg, A. 2005, AN, 326, 787, doi: 10.1002/asna.200510414

Brandenburg, A., Rädler, K. H., & Kemel, K. 2012, A&A, 539, A35, doi: 10.1051/0004-6361/201117871

Brandenburg, A., Rädler, K.-H., & Schrinner, M. 2008, A&A, 482, 739, doi: 10.1051/0004-6361:200809365

Brandenburg, A., Schober, J., & Rogachevskii, I. 2017, AN, 338, 790, doi: 10.1002/asna.201713384

Brandenburg, A., & Sokoloff, D. 2002, GApFD, 96, 319, doi: 10.1080/03091920290032974

Brandenburg, A., Svedin, A., & Vasil, G. M. 2009, MNRAS, 395, 1599, doi: 10.1111/j.1365-2966.2009.14646.x

Chkhetiani, O. G., Hnatich, M., Jurčišinová, E., et al. 2006, PhRvE, 74, 036310, doi: 10.1103/PhysRevE.74.036310

de Avillez, M. A., & Mac Low, M.-M. 2002, ApJ, 581, 1047, doi: 10.1086/344256

Devlen, E., Brandenburg, A., & Mitra, D. 2013, MNRAS, 432, 1651, doi: 10.1093/mnras/stt590

Dolginov, A. Z., & Silant'ev, N. A. 1987, Zh. Eksp. Teor. Fiz., 93, 159

Elperin, T., Kleeorin, N., & Rogachevskii, I. 1997, Phys. Rev. E, 55, 2713, doi: 10.1103/PhysRevE.55.2713

Furutsu, K. 1963, J. Res. Natl Bureau Standards – D. Radio Propagation, 67D, 303323

Haugen, N. E. L., Kleeorin, N., Rogachevskii, I., & Brandenburg, A. 2012, PhFl, 24, 075106

Hubbard, A., & Brandenburg, A. 2009, ApJ, 706, 712, doi: 10.1088/0004-637X/706/1/712

Jabbari, S., Brandenburg, A., Losada, I. R., Kleeorin, N., & Rogachevskii, I. 2014, A&A, 568, A112, doi: 10.1051/0004-6361/201423499

Käpylä, P. J., & Singh, N. K. 2022, JFM, 952, R1, doi: 10.1017/jfm.2022.906

Kishore, G., & Singh, N. K. 2025, ArXiv:2502.02946

Mitra, D., Käpylä, P. J., Tavakol, R., & Brandenburg, A. 2009, A&A, 495, 1, doi: 10.1051/0004-6361:200810359

Mizerski, K. A. 2023, PhRvE, 107, 055205, doi: 10.1103/PhysRevE.107.055205

Nicklaus, B., & Stix, M. 1988, GApFD, 43, 149, doi: 10.1080/03091928808213623

Novikov, E. A. 1965, JETP, 20, 1290

Pencil Code Collaboration, Brandenburg, A., Johansen, A., et al. 2021, J. Open Source Softw., 6, 2807, doi: 10.21105/joss.02807

Rädler, K.-H., Brandenburg, A., Del Sordo, F., & Rheinhardt, M. 2011, PhRvE, 84, 046321, doi: 10.1103/PhysRevE.84.046321

Rädler, K.-H., Kleeorin, N., & Rogachevskii, I. 2003, GApFD, 97, 249, doi: 10.1080/0309192031000151212

Rheinhardt, M., & Brandenburg, A. 2012, AN, 333, 71, doi: 10.1002/asna.201111625

Rogachevskii, I. 2021, Introduction to turbulent transport of particles, temperature and magnetic fields: analytical methods for physicists and engineers (Cambridge University Press), doi: 10.1063/5.0188732,2024

Rogachevskii, I., Kleeorin, N., & Brandenburg, A. 2018, JPlPh, 84, 735840502, doi: 10.1017/S0022377818000983

Rogachevskii, I., Kleeorin, N., & Brandenburg, A. 2025, ApJ, submitted; arXiv:2501.13807, doi: 10.48550/arXiv.2501.13807

Rüdiger, G. 1989, Differential rotation and stellar convection. Sun and the solar stars (Berlin: Akademie Verlag)

Schober, J., Rogachevskii, I., Brandenburg, A., et al. 2018, ApJ, 858, 124, doi: 10.3847/1538-4357/aaba75

Schrinner, M., Rädler, K.-H., Schmitt, D., Rheinhardt, M., & Christensen, U. 2005, AN, 326, 245, doi: 10.1002/asna.200410384

Schrinner, M., Rädler, K.-H., Schmitt, D., Rheinhardt, M., & Christensen, U. R. 2007, GApFD, 101, 81, doi: 10.1080/03091920701345707

Sur, S., Brandenburg, A., & Subramanian, K. 2008, MNRAS, 385, L15, doi: 10.1111/j.1745-3933.2008.00423.x

Zhou, Y. 1990, PhRvA, 41, 5683, doi: 10.1103/PhysRevA.41.5683